Available online at www.sciencedirect.com
ScienceDirect
Journal of Luminescence 125 (2007) 175–183
JOURNAL OF LUMINESCENCE
www.elsevier.com/locate/jlumin

Theoretical studies of electron-vibrational $4f^N$–$4f^{N-1}5d$ spectra in $LiYF_4$:RE^{3+} crystals

B.Z. Malkin*, O.V. Solovyev, A.Yu. Malishev, S.K. Saikin

Department of Physics, Kazan State University, Kremlevskaya 18, 420008 Kazan, Russian Federation

Available online 7 September 2006

Abstract

The UV and VUV inter-configuration $4f^N$–$4f^{N-1}5d$ spectra of rare-earth ions in insulators consist of broad electron-vibrational bands which sometimes have a resolved fine structure. In the present work, the low-temperature absorption band shapes of the impurity Ce^{3+}, Pr^{3+} and Nd^{3+} ions in $LiYF_4$ crystals have been simulated in the framework of the microscopic theory operating with the real phonon spectrum of the host crystal lattice. The energy levels and wave functions of the ground ($4f^N$) and excited ($4f^{N-1}5d$) electronic configurations of rare-earth ions were obtained from the numerical diagonalization of the Hamiltonian containing energies of electrostatic Coulomb and exchange interactions between electrons, spin–orbit interactions and the crystal field interaction. Crystal field parameters and electron–phonon coupling constants were treated in the framework of the exchange charge model. Form-functions of the spectral bands proportional to the calculated integral intensities of electric dipole transitions are obtained as a sum of convolutions of spectral densities of multiphonon correlation functions and form-functions of zero-phonon lines with the widths determined by distributions of random lattice strains and non-radiative transition probabilities. The calculated values of the Huang–Rhys parameters of crystal field states in mixed $4f^{N-1}5d$ configurations vary in the range from 0.1 to 15 and correspond to intermediate or strong electron–phonon interactions. Results of simulations of the spectral envelopes agree satisfactorily with the experimental data available from the literature.

PACS: 71.70.−d; 78.20.Bh; 78.40.Ha

Keywords: 4f–5d spectra; electron–phonon interaction; $LiYF_4$

1. Introduction

Studies of spectral properties and excitation dynamics in rare-earth-doped crystals allow to test theories of the electron–lattice interaction at different regimes of coupling strength (weak in the ground $4f^N$ electronic configuration and strong in the excited $4f^{N-1}5d$ configuration). Investigations of mixed $4f^{N-1}5d$ configurations started from the pioneer works by Feofilov [1] and Kaplyanskii and Feofilov [2] on the spectra of impurity divalent rare-earth ions in alkaline-earth fluorides. The quantitative features of the structural form of electron-vibrational $4f^N$–$4f^{N-1}5d$ spectra for divalent rare-earth ions in alkali-halides were discussed by Wagner and Bron [3] using a simplified model of electron–lattice interaction. As it has been shown by Kaplyanskii and Przhevuskii [4] by piezo-spectroscopic measurements, deformation potentials of $4f^{N-1}5d$ states exceed ones for $4f^N$ states by an order of magnitude.

New possibilities of taking VUV spectra with the use of synchrotron radiation demonstrated by Yen et al. [5,6] were widely explored during last 10 years. Systematic experimental studies of the $4f^N$–$4f^{N-1}5d$ excitations and respective $4f^{N-1}5d$–$4f^N$ emission, theoretical modeling of energy-level patterns and transition intensities in the $4f^N$–$4f^{N-1}5d$ spectra were carried out for a lot of systems. Trends in the atomic parameters were systematized by Reid et al. [7]. An original theory of 4f–5d spectra of impurity rare-earth ions based on simulations of molecular orbitals in large clusters of ions in dielectric crystals was derived by Ogasawara et al. [8].

*Corresponding author. Tel.: +7 8432 315342; fax: +7 8432 387418.
E-mail address: Boris.Malkin@ksu.ru (B.Z. Malkin).

0022-2313/$ - see front matter © 2006 Elsevier B.V. All rights reserved.
doi:10.1016/j.jlumin.2006.08.011

Most of the intensity in the f–d transitions is in broad vibronic bands with widths up to a thousand of wave numbers even at the liquid helium temperature contrary to the sharp zero-phonon lines with widths less than 10 wave numbers in the intra-configuration f–f spectra. To reproduce the observed spectra, three adjustable parameters are used: the offset, the bandwidth and the intensity ratio of the zero-phonon line to the vibronic band. Gaussian-shaped bands are usually superimposed on the zero-phonon lines. An attempt was done to simulate the real shape of the 4f–5d spectrum by Liu et al. [9]. The spectral function for the emission spectrum 5d–4f($^2F_{5/2}$) of Ce^{3+} in Cs_2NaYCl_6 was fitted to the measured spectrum. However, the theoretical model is essentially phenomenological and needs a number of fitting parameters (frequencies of effective vibrations, effective widths of local mode), and for the lattice vibrational spectrum as well as for Huang–Rhys parameters for each local mode and for the lattice continuous band.

In this work, we compute the low-temperature absorption spectra of Ce^{3+}, Pr^{3+}, and Nd^{3+} ions in $LiYF_4$ and compare theoretical results with the experimental data. All concrete calculations are fulfilled for $T=0$ in the framework of the cluster approximation (only vibrations of the impurity ion and its nearest neighbors are taken into account).

2. Theory of the optical band shapes

The form-function of the optical spectrum related to the radiative transition between the non-degenerate electronic states Γ and Γ' of an impurity rare-earth ion in a dielectric crystal is given by the Fourier integral

$$F_{\Gamma\Gamma'}(\Omega)=\frac{1}{\hbar^2}\int_{-\infty}^{\infty} I_{\Gamma\to\Gamma'}(t)\exp\left[-\mathrm{i}(\omega^0_{\Gamma\Gamma'}-\Omega)t\right]\mathrm{d}t, \tag{1}$$

where Ω is the frequency of the emitted light, $\hbar\omega^0_{\Gamma\Gamma'}=E(\Gamma)-E(\Gamma')>0$ is the energy gap between the considered electronic energy levels in the static crystal lattice, and in the framework of the adiabatic approximation the generating function has the form [10]

$$I_{\Gamma\Gamma'}(t)=\mathrm{Sp}_{\mathrm{ph}}\Big[(\boldsymbol{d\varepsilon})_{\Gamma\Gamma'}\exp(\mathrm{i}tH^{\Gamma'}_{\mathrm{ph}}/\hbar)(\boldsymbol{d\varepsilon})^{+}_{\Gamma\Gamma'} \times\exp(-\mathrm{i}tH^{\Gamma}_{\mathrm{ph}}/\hbar)\rho^{\Gamma}_{\mathrm{ph}}\Big]. \tag{2}$$

The spectral distribution of the emitted energy is proportional to $\Omega^4F_{\Gamma\Gamma'}(\Omega)$. Here $(\boldsymbol{d\varepsilon})_{\Gamma\Gamma'}$ is the matrix element of the projection of the effective electric dipole moment $\boldsymbol{d}$ of an ion on the polarization vector $\boldsymbol{\varepsilon}$ of the radiation (we use the Condon approximation [11] and neglect the dependence of the electric dipole moment, responsible for the interaction of electrons with the electromagnetic field, on lattice variables), $\rho^{\Gamma}_{\mathrm{ph}}$ is the equilibrium density matrix of the phonon subsystem corresponding to the electronic state Γ with the Hamiltonian

$$H^{\Gamma}_{\mathrm{ph}}=<\Gamma|H_{\mathrm{el-ph}}|\Gamma>+\sum_f\hbar\omega^{(\Gamma)}_f\left[n(\omega_f)+\tfrac{1}{2}\right], \tag{3}$$

the sum is taken over lattice normal modes with frequencies $\omega_f^{(\Gamma)}$ and occupation numbers $n(\omega_f)$, and $H_{\mathrm{el-ph}}$ is the Hamiltonian of the electron–phonon interaction. The latter can be written as a power series in differences $\boldsymbol{u}(Ls,R)=\boldsymbol{u}(Ls)-\boldsymbol{u}(R)$ between dynamical displacements (which are linear in normal mode coordinates) of host ions (unit cells and ions in the cell are labeled by L and s, respectively) and the rare-earth ion (R) from their equilibrium positions $\boldsymbol{R}_{Ls}$, $\boldsymbol{R}_{\boldsymbol{0}}$ in the lattice

$$\begin{aligned}H_{\mathrm{el-ph}}=&\sum_{\alpha,Ls}V_\alpha(Ls)u_\alpha(Ls,R)\\&+\frac{1}{2}\sum_{\alpha\beta,Ls}V_{\alpha\beta}(Ls)u_\alpha(Ls,R)u_\beta(Ls,R)+\cdots\\&+\frac{1}{n!}\sum_{\alpha_1\ldots\alpha_n,Ls}V_{\alpha_1\ldots\alpha_n}(Ls)u_{\alpha_1}(Ls,R)\ldots u_{\alpha_n}(Ls,R)\\&+\cdots\end{aligned} \tag{4}$$

The coefficients in Eq. (4) are the electronic operators. In the framework of the crystal field theory, we can write these one-particle operators projected on the subspace of states of the electronic $(nl)^N$ configuration through the spherical tensor operators $C^{(p)}_k$

$$\begin{aligned}V_\alpha(Ls)&=\sum_{pk}B^p_{k,\alpha}(Ls)C^{(p)}_k,\ V_{\alpha\beta}(Ls)\\&=\sum_{pk}B^p_{k,\alpha\beta}(Ls)C^{(p)}_k,\ldots,\end{aligned} \tag{5}$$

where $B^p_{k,\alpha}(Ls)$, $B^p_{k,\alpha\beta}(Ls)\ldots$ are the coupling constants (Cartesian components of vectors are labeled by Greek indices); values of coupling constants depend on the concrete principal (n) and orbital (l) quantum numbers. In accordance with the definition (3) of the effective phonon Hamiltonian, we have to consider only adiabatic (diagonal in respect the electronic states) terms in the Hamiltonian (4).

Accounting only for the linear electron–phonon coupling (the first term in Eq. (4)) and neglecting changes in phonon frequencies in different electronic states, it is possible to obtain the following form of the generating function [12]

$$I_{\Gamma\Gamma'}(t)=(\boldsymbol{d\varepsilon})_{\Gamma\Gamma'}(\boldsymbol{d\varepsilon})_{\Gamma'\Gamma}\exp\left[M^{\Gamma'}_{\Gamma}(t)-M^{\Gamma'}_{\Gamma}(0)\right] \times\exp[-\mathrm{i}(E_{\mathrm{JT}}(\Gamma)-E_{\mathrm{JT}}(\Gamma'))t]. \tag{6}$$

Here,

$$M^{\Gamma'}_{\Gamma}(t)=\frac{1}{\pi\hbar}\int D_{\Gamma\Gamma'}(\omega)\left[\mathrm{e}^{\mathrm{i}\omega t}(n(\omega)+1) +\mathrm{e}^{-\mathrm{i}\omega t}n(\omega)\right]\mathrm{d}\omega/\omega^2, \tag{7}$$

$$D_{\Gamma\Gamma'}(\omega)=\sum_{\alpha\beta LsL's'}\left([V_\alpha(Ls)]_{\Gamma\Gamma}-\left[V_\alpha(Ls)\right]_{\Gamma'\Gamma'}\right)\times g_{\alpha\beta}(Ls,L's'|\omega)\left(\left[V_\beta(L's')\right]_{\Gamma\Gamma}-\left[V_\beta(L's')\right]_{\Gamma'\Gamma'}\right), \tag{8}$$

and

$$E_{\rm JT}(\Gamma)=-\frac{1}{\pi}\int[V_\alpha(Ls)]_{\Gamma\Gamma}g_{\alpha\beta}(Ls,L's'|\omega)_{\Gamma\Gamma}\times\left[V_\beta(L's')\right]_{\Gamma\Gamma}/\omega \tag{9}$$

is the Jahn–Teller energy (the shift of the electron energy due to the electron–phonon coupling). In Eq. (8), $g_{\alpha\beta}(Ls,L's'|\omega)$ is the spectral density of the lattice advanced Green's function $\langle\langle u_\alpha(Ls,R|t),u_\beta(L's',R|0)\rangle\rangle$ for relative dynamic displacements of the rare earth and host ions

$$g_{\alpha\beta}(Ls,L's'|\omega)=\mathrm{Im}\left[G_{\alpha\beta}(Ls,L's'|\omega)-G_{\alpha\beta}(Ls,R|\omega)-G_{\alpha\beta}(R,L's'|\omega)+G_{\alpha\beta}(R,R|\omega)\right], \tag{10}$$

$$\mathrm{Im}\,G^0_{\alpha\beta}\left(Ls,L's'\right|\omega)=\frac{\pi}{N\sqrt{m_sm_{s'}}}\times\sum_{\mathbf{q}j}e_\alpha(\boldsymbol{qj}|s)e_\beta(\boldsymbol{qj}|s')^*\exp[\mathrm{i}\boldsymbol{q}(\boldsymbol{R}_{Ls}-\boldsymbol{R}_{L's'})]\times\delta\left(\omega^2-\omega_j^2(\boldsymbol{q})\right), \tag{11}$$

where m_s is the ion mass, $\boldsymbol{e}(\boldsymbol{qj}|s)$ is the polarization vector for the ion s in the lattice normal mode with the wave vector $\boldsymbol{q}$ and the frequency $\omega_j(\boldsymbol{q})$ from the branch j of the phonon spectrum, N is the number of vectors $\boldsymbol{q}$ in the Brillouin zone.

As it follows from Eq. (6), probability of any transition between electronic states Γ and Γ' contains the Debye–Waller factor $\exp[-M_\Gamma^{\Gamma'}(0)]$ that accounts for the overlap between wave functions of lattice oscillators related to different adiabatic potentials. At zero temperature the Debye–Waller factor can be expressed through the Huang–Rhys parameter

$$S(\Gamma\Gamma')=M_\Gamma^{\Gamma'}(0,T=0)=\frac{1}{\pi\hbar}\int D_{\Gamma\Gamma'}(\omega)\,\mathrm{d}\omega/\omega^2. \tag{12}$$

The dependence of the generating function $I_{\Gamma\to\Gamma'}(t)$ on its argument is determined by the factor $\exp\left[M_\Gamma^{\Gamma'}(t)-M_\Gamma^{\Gamma'}(0)\right]$. Expanding the exponent in a power series in $M_\Gamma^{\Gamma'}(t)$, and collecting terms with $1,\ \mathrm{e}^{\pm\mathrm{i}\omega t}\mathrm{e}^{\pm\mathrm{i}(\omega_1t\pm\omega_2t)},\ldots$, it is possible to present the form-function as a sum of spectra corresponding to p-phonon transitions ($p=0,1,2\ldots$). In particular, neglecting phonon occupation numbers at low temperatures, we obtain the following emission form-function which corresponds to simultaneous emission of a photon and creation of one, two, …p, … phonons:

$$F_{\Gamma\Gamma'}(\Omega)=2\pi\frac{|(\boldsymbol{d\varepsilon})_{\Gamma\Gamma'}|^2}{\hbar^2}\mathrm{e}^{-S(\Gamma\Gamma')}\sum_{p=0}^{\infty}M_{p,\Gamma\Gamma'}(\omega_{\Gamma\Gamma'}-\Omega), \tag{13}$$

here $\hbar\omega_{\Gamma\Gamma'}=\hbar\omega^0_{\Gamma\Gamma'}+E_{\rm JT}(\Gamma)-E_{\rm JT}(\Gamma')$ is the difference between the minima of the adiabatic potentials in the states Γ and Γ', and

$$M_{p,\Gamma\Gamma'}(\omega_{\Gamma\Gamma'}-\Omega)=\frac{1}{(\pi\hbar)^p p!}\int D_{\Gamma\Gamma'}(\omega_1)\ldots D_{\Gamma\Gamma'}(\omega_p)\times\delta(\omega_{\Gamma\Gamma'}-\omega_1-\ldots-\omega_p-\Omega)\,\frac{\mathrm{d}\omega_1}{\omega_1^2}\cdots\frac{\mathrm{d}\omega_p}{\omega_p^2}. \tag{14}$$

The absorption cross-section is proportional to $\Omega F_{\Gamma\Gamma'}(\Omega)$ with the inverted signs of Ω and $\omega_{\Gamma\Gamma'}$. The value of $\Omega=\omega_{\Gamma\Gamma'}$ presents a singular point of the form-function ($M_0(\omega)=\delta(\omega)$) that corresponds to the zero-phonon line with the integral intensity determined by the Debye–Waller factor [13]. All spectral distributions (14) with $p>1$ can be simulated using the recurrent relations ($\omega_{\rm M}$ is the maximum phonon frequency) [14]

$$M_1(\omega)=\frac{1}{(\pi\hbar)}D_{\Gamma\Gamma'}(\omega)\frac{1}{\omega^2}, \tag{15}$$

$$M_p(0<\omega<\omega_{\rm M})=\frac{1}{p}\int_0^{\omega}M_1(\omega_1)M_{p-1}(\omega-\omega_1)\,\mathrm{d}\omega_1\quad(p>1), \tag{16a}$$

$$M_p(\omega_{\rm M}<\omega<(p-1)\omega_{\rm M})=\frac{1}{p}\int_0^{\omega_{\rm M}}M_1(\omega_1)M_{p-1}(\omega-\omega_1)\,\mathrm{d}\omega_1\quad(p>2), \tag{16b}$$

$$M_p((p-1)\omega_{\rm M}<\omega<p\omega_{\rm M})=\frac{1}{p}\int_{\omega-(p-1)\omega_{\rm M}}^{\omega_{\rm M}}M_1(\omega_1)M_{p-1}(\omega-\omega_1)\,\mathrm{d}\omega_1\quad(p>1). \tag{16c}$$

The form-function (13) contains an infinite number of terms corresponding to multi-phonon optical transitions. However, a relative weight of a p-phonon band presented by the spectral distribution $M_{p,\Gamma\Gamma'}(\omega_{\Gamma\Gamma'}-\Omega)$ with an increasing number p of phonons involved reaches a maximum value for $p\approx S(\Gamma\Gamma')$ and after that relatively quickly diminishes. Thus, the number $N_{\rm b}$ of bands which we have to consider depends on the value of the Huang–Rhys parameter for a transition, really it is enough to include $N_{\rm b}\leqslant 2S(\Gamma\Gamma')$ bands. The infinite lattice sum in expression (8) may be simplified when taking into account interactions between the rare-earth ion and its nearest neighbors only. For values of $S(\Gamma\Gamma')$ less or comparable to unity, the one-phonon band (15) plays a dominant role, and a spectrum has a fine structure that reflects the specific features of the phonon density of states projected on the relative displacements of the impurity ion and its ligands. With the increasing order of a band, this fine structure is quickly smoothed out. It should be noted that shapes of p-phonon bands for large values of p (actually, for $p>5$) may be well approximated by Gaussians of appropriate widths connected by the scaling transformations

$$M_p(\omega)\sim\frac{1}{(\pi\Delta^2p)^{1/2}}\exp\left[-\frac{(\omega-\omega_{\rm eff}p)^2}{\Delta^2p}\right], \tag{17}$$

$\omega_{\rm eff}$ may be considered as the frequency of the most effective adiabatic phonon coupled to the electron localized at the rare-earth ion.

Thus, we have a possibility to simulate the spectral envelopes by carrying out calculations of energies and wave functions of the electronic subsystem in the static crystal field, spectral densities of the lattice Green's functions for a cluster containing the rare-earth ion and its ligands, linear coupling constants in the Hamiltonian of the electron–phonon interaction and matrix elements of the electron radius vector. At the last step we have to account for a distribution of electron energies due to random lattice strains (inhomogeneous broadening) and finite lifetimes of the excited states (relaxation broadening).

3. Simulations of $4f^N$–$4f^{N-1}5d$ absorption spectra in $LiYF_4$:RE^{3+} crystals

Impurity rare-earth ions substitute for Y^{3+} ions in $LiYF_4$ crystals (C_{4h}^6 space group) in sites with the S_4 point symmetry. In the nearest surroundings of the Y-site, there are eight fluorine ions which form two deformed tetrahedrons. In the crystallographic system of coordinates with its origin on the rare-earth ion, ligand coordinates are $(x_k\ y_k\ z_k)$, $(-x_k\ -y_k\ z_k)$, $(y_k\ -x_k\ -z_k)$, $(-y_k\ x_k\ -z_k)$, $k=1,2$. In the perfect lattice, four fluorine ions are at the distance $R_1=0.2297$ nm from the rare-earth ion ($x_1=0.1645a$, $y_1=0.2183a$, $z_1=-0.1687c$, here $a=0.5164$ nm, $c=1.0741$ nm are the lattice constants), and four other fluorine ions are at the distance $R_2=0.2244$ nm ($x_2=x_1-0.5a$, $y_2=y_1$, $z_2=-z_1-0.25c$) [15].

The vibrational spectrum of the $LiYF_4$ crystal lattice was studied by Salaun et al. [16,17]. Results of optical and neutron inelastic-scattering experiments were described successfully in the framework of the rigid-ion model. The maximum phonon frequency $\omega_{\rm M}$ of this crystal equals 560 cm^{-1}. Using parameters of this model, we computed frequencies and polarization vectors of vibrations for 8870 wave vectors distributed uniformly over the irreducible part of the Brillouin zone. Imaginary parts of the lattice Green's functions (11) for the relative displacements of Y^{3+} ion and its nearest neighbors were calculated at the equally spaced 1120 points ω_f ($0\leqslant\omega_f\leqslant\omega_{\rm M}$) on the frequency axis by numerical integration over the Brillouin zone. Examples of the calculated spectral densities of the displacement–displacement correlation functions were given in Refs. [18,19].

Energy-level patterns of mixed $4f^{N-1}5d$ configurations in rare-earth-doped $LiYF_4$ crystals were thoroughly studied in Refs. [20–24]. We used the same procedure and obtained energies and wave functions of all states of the $4f^{N-1}5d$ and $4f^N$ configurations of Ce^{3+} ($N=1$), Pr^{3+} ($N=2$), Nd^{3+} ($N=3$) from the numerical diagonalization of the Hamiltonian

$$H=H_o+H_{ee}(4f4f)+H_{ee}(4f5d)+H_{\rm SO}(4f)+H_{\rm CF}(4f)+H_{\rm SO}(5d)+H_{\rm CF}(5d) \quad (18)$$

which contained the shift H_0 of the excited configuration relative to the ground one, electrostatic interactions between electrons, spin–orbit interactions and crystal field energies. Configuration interactions were neglected, and the ground and excited configurations were considered independently. The initial values of Slater parameters $F^{(k)}$(4f, 4f), $F^{(k)}$(4f, 5d), $G^{(k)}$(4f, 5d) and spin–orbit coupling constants ζ(4f) and ζ(5d) were taken from Refs. [20–24], the crystal field was considered in the framework of the exchange charge model [25] with parameters fitted to the experimental data. The crystal field affects the 5d-electron essentially stronger than the 4f electron with the much more contracted space distribution. We have neglected the interaction of 4f electrons with phonons as compared with the 5d-electron–phonon coupling in the mixed configurations, and below we limit ourselves by a description of calculations of crystal field parameters in the Hamiltonian $H_{\rm CF}(5d)=\sum_{pk}B_k^p(5d)C_k^{(p)}$ for the 5d-electron only. These parameters determine the energy of the 5d-electron (averaged with the 5d-radial wave function) in the fields of point and exchange charges. In a case of filled outer electronic ns^2, np^6 shells of ligands,

$$B_k^p(5d)=e^2\sum_L\left\{-q_L<5d|r^p|5d>k_p+\frac{2(2p+1)}{5}R_L^pS_p^{(5d)}(R_L)\right\}\times(-1)^kC_{-k}^{(p)}(\vartheta_L,\varphi_L)/R_L^{p+1}, \quad (19)$$

where the sum is taken over all ions in the host lattice with charges eq_L and the spherical coordinates R_L, θ_L, φ_L; the field of exchange charges is defined by quadratic forms of the overlap integrals $<5dl_z|nll_z>$ [25] ($S_s(R_L)=<5d0|ns0>$, $S_\sigma(R_L)=<5d0|np0>$, $S_\pi(R_L)=<5d1|np1>$)

$$S_p^{(5d)}(R_L)=G_sS_s^2+G_\sigma S_\sigma^2+\gamma_pG_\pi S_\pi^2,\quad \gamma_2=1,\quad \gamma_4=-4/3; \quad (20)$$

k_p, G_s, G_σ, G_π are the phenomenological parameters of the model (the coefficient k_p has been introduced to account for the electrostatic interaction between the overlapping electron densities of ligands and the 5-d electron). The moments of the 5d-electron density and overlap integrals were calculated using analytical radial 5d functions of divalent and trivalent rare-earth ions presented in [26,27] and the 2s, 2p functions of the F^- ion from Ref. [28], the dependences of overlap integrals on the distance between the rare earth and the F^- ion were approximated by polynomials of second order $S(R_L)=a+bR_L+cR_L^2$ for $0.22<R_L<0.26$ nm (see Table 1). Values of the parameters $k_2=1/2$, $k_4=1$, $Gs=1.15$, $G_\sigma=G_\pi=1.3$, the f–d excitation energies H_0 (44,450; 49,770; 53,330 cm^{-1} for Ce^{3+}, Pr^{3+}, Nd^{3+}, respectively), atomic parameters (see Table 2) were obtained from the self-consistent fitting of the calculated spectra to the experimental data (ion charges q_L were fixed as -1 (F^-), $+1$ (Li^+), $+3$ (Y^{3+})). Radial expansion of the coordination shells by 3.6% and 3%

Table 1
Overlap integrals for the rare-earth ion 5d and the fluorine ion 2s, 2p functions, and 5d-electron radial moments

	Ce^{3+}	Pr^{3+}	Nd^{3+}
a_s	1.3612	1.3491	1.3370
b_s (nm^{-1})	−8.056	−7.998	−7.94
c_s (nm^{-2})	12.35	12.29	12.22
a_σ	0.1553	0.1666	0.1780
b_σ (nm^{-1})	0.9803	0.8683	0.7562
c_σ (nm^{-2})	−4.233	−3.992	−3.751
a_π	1.0551	1.0476	1.0402
b_π (nm^{-1})	−6.499	−6.462	−6.425
c_π (nm^{-2})	10.47	10.42	10.38
$<5d\|r^2\|5d>$ (nm^2)	1.5782×10^{-2}	1.5326×10^{-2}	1.4911×10^{-2}
$<5d\|r^4\|5d>$ (nm^4)	3.8628×10^{-4}	3.66×10^{-4}	3.48×10^{-4}

Table 2
Parameters (cm^{-1}) used in the calculations of crystal field energies and wave functions of impurity rare-earth ions in $LiYF_4$

	Ce^{3+}		Pr^{3+}		Nd^{3+}	
	4f	5d	$4f^2$	4f5d	$4f^3$	$4f^25d$
$F^{(2)}$	—	—	68878 (ff)	21000 (fd)	73519 (ff)	20852 (fd)
$F^{(4)}$	—	—	50347 (ff)	15939 (fd)	53143 (ff)	15752 (fd)
$F^{(6)}$	—	—	32901 (ff)	—	34924 (ff)	—
$G^{(1)}$	—	—	—	10115 (fd)	—	10043 (fd)
$G^{(3)}$	—	—	—	11812 (fd)	—	11691 (fd)
$G^{(5)}$	—	—	—	8616 (fd)	—	8515 (fd)
ζ(4f)	625	—	752	780	885	885
ζ(5d)	—	1082	—	1062	—	1124
B_0^2	360	4678	433	(5d) 4692	372	(5d) 4728
B_0^4	−1400	−18008	−1068	(5d)-17752	−974	(5d)-17528
B_4^4	−1240	−16722	−1145	(5d)-16512	−1116	(5d)-16293
	+751i	+16949i	+655i	+16741i	+598i	+16506i
B_0^6	−67.2	—	−67	—	−20	—
B_4^6	−1095	—	−1095	—	−1020	—
	+458i		+458i		+200i	

(Ce^{3+}); 3 and 2.5% (Pr^{3+}); 2.5% and 2% (Nd^{3+}) for the nearest and the next-nearest ligands, respectively) was taken into account [29,30]. To describe the crystal fields affecting 4f electrons in the both ground and excited configurations of Pr^{3+} and Nd^{3+}, we used parameters B_k^p(4f) given in Refs. [31] and [32], respectively.

Analytical expressions of the linear coupling constants in the Hamiltonian of the 5d-electron–phonon interaction were obtained by direct differentiation of functions (19) with respect to the 24 coordinates of eight ligands. The variation of the crystal field due to the ligand L displacement along the crystallographic α-axis is determined by 14 coupling constants $B^p_{k,\alpha}(L)$ ($p = 2,4$). Values of a total number of 24×14 coupling constants were calculated using the above given parameters of the crystal field model. The computed matrices of the electronic operators $V_\alpha(L)$ in the basis of the eigenfunctions of the Hamiltonian (18) were used to calculate Huang–Rhys parameters (12) and Jahn–Teller energies (9) for all crystal field states of the considered $4f^{N-1}5d$ configurations. Because we can neglect the electron–phonon interaction in the $4f^N$ configuration, all band shapes of transitions between the fixed state in the excited $4f^{N-1}5d$ configuration and any state in the $4f^N$ configuration are the same, only relative integral intensities of these bands vary in accordance with the corresponding matrix elements of the electronic dipole moment ($d_x = \Sigma ex$ and $d_z = \Sigma ez$ for the σ- and π-polarized radiation, respectively).

To estimate the relaxation broadening of the $4f^N$–$4f^{N-1}5d$ transitions, we calculated probabilities of the spontaneous one-phonon transitions from each $4f^{N-1}5d$ state

$$W_{\Gamma\to\Gamma'} = \frac{2}{\hbar}\sum_{Ls\alpha L's'\beta}[V_\alpha(Ls)]_{\Gamma'\Gamma}g_{\alpha\beta}(Ls,L's'|\omega_{\Gamma\Gamma'}) \times[V_\beta(L's')]_{\Gamma\Gamma'}(n(\omega_{\Gamma\Gamma'})+1) \quad (21)$$

induced by non-adiabatic phonons. These transitions are allowed only between the states with the energy gap less than the maximum phonon energy. The average gap between the energy levels in the $4f^{N-1}5d$ configuration quickly diminishes with the increasing number N of electrons in the ground configuration (there are five Kramers doublets with the average gap of more than $4000\,cm^{-1}$ in the spectrum of Ce^{3+}, the energy-level pattern of the 4f5d (Pr^{3+}) configuration contains 70 singlets and 35 non-Kramers doublets with the average gap of $290\,cm^{-1}$, in the spectrum of the $4f^25d$ (Nd^{3+}) configuration the average gap between 455 Kramers doublets diminishes up to $160\,cm^{-1}$), and the role of the non-adiabatic coupling becomes dominant. The calculated line widths $\hbar W_{\Gamma\to\Gamma'}$ for a number of states in the $4f^{N-1}5d$ configurations ($N>1$) are comparable or even essentially larger than the energy gap $\hbar\omega_{\Gamma\Gamma'}$. This means that the corresponding states Γ and Γ' cannot be considered in the framework of the adiabatic approximation, and we should search for a spectral distribution of mixed electron–phonon states (the same problem arises in a case of non-Kramers doublet levels). However, we can estimate widths of these distributions from calculations of transition probabilities (21), or the Jahn–Teller energies (9) where we have to substitute $[V_\alpha(Ls)]_{\Gamma\Gamma'}$ for $[V_\alpha(Ls)]_{\Gamma\Gamma}$. Thus, at the last step of simulations, the computed form-functions (13) were convoluted with the Gaussian to take into account the inhomogeneous broadening (we assumed the corresponding width of $30\,cm^{-1}$) and with the Lorentzian to take into account the relaxation broadening and the spectral distribution of electron–phonon excitations. Results of simulations are presented in Figs. 1–7.

4. Discussion and conclusions

The very first analysis of the 4f–5d absorption spectrum in the simplest system (Ce^{3+}) has revealed general features of absorption and excitation spectra in $LiYF_4$ crystals

containing different rare-earth ions. In Table 3, we present the calculated crystal field energies of the 5d-electron (column 1), the shifts of the electronic energies due to coupling with the adiabatic phonons (column 2), frequencies of zero-phonon lines in the absorption spectrum from the ground state (column 3, GSA, the lowest frequency was fitted to the measured value), positions of the maxima of the simulated bands (column 4) in comparison with the experimental data (column 5), the Huang–Rhys parameters $S(\Gamma)$ (column 6), and the relative integral intensities of the σ- and π-polarized bands (columns 7 and 8). In accordance with the available experimental data [33,34], the lowest band in GSA is mainly σ-polarized, while the next band is π-polarized. The calculated (with making use of the crystal field parameters $B_k^p(4f)$ given in Table 2) crystal field energies of the 4f electron 0; 242 (216); 514; 2222 (2221); 2320 (2316); 2432 (2430); 3121 (3160) cm^{-1} and g-factors of the ground state $g_{||} = 2.846$ (2.765), $g_{\perp} = 1.552$ (1.473) are consistent with the literature data (presented in brackets) [34,35]. As it follows from results of calculations (see Table 3), the lowest 5d state is relatively weakly coupled to phonons. The similar results are obtained for the lowest states in the 4f5d and $4f^2$5d configurations (with the Huang–Rhys parameters of 3.27 and 2.725, and the Jahn–Teller energies of 760 and 540 cm^{-1}, respectively). For the next well-separated 5d-state the Huang–Rhys parameter has its maximum value. It is worthy noting that the p-phonon spectral densities have the maximum values at frequencies $p\omega_{\rm eff}(\Gamma)$ (see Eq. (17)), and the frequencies of the most effective lattice vibrations $\omega_{\rm eff}(\Gamma)$ close to 200 cm^{-1} are much smaller than the maximum phonon frequency $\omega_{\rm M} = 560\,cm^{-1}$. The shift of the maximum of the form-function $F_{\Gamma\Gamma'}(\Omega)$ from the corresponding zero-phonon line can be approximated by $S(\Gamma)\omega_{\rm eff}(\Gamma) \sim -E_{\rm JT}(\Gamma)$. The upper three 5d-states (the orbital doublet split by the spin–orbit interaction and the orbital singlet) form a group of closely spaced levels, and the third and fourth absorption bands are superimposed on each other (see the dashed curve in Fig. 1). The peaks close to 50,000 cm^{-1} observed in the experimental excitation spectra [21,36] become resolved in the simulated envelope after taking into account the mutual repulsion between the components of the orbital doublet strongly mixed by the non-adiabatic phonons.

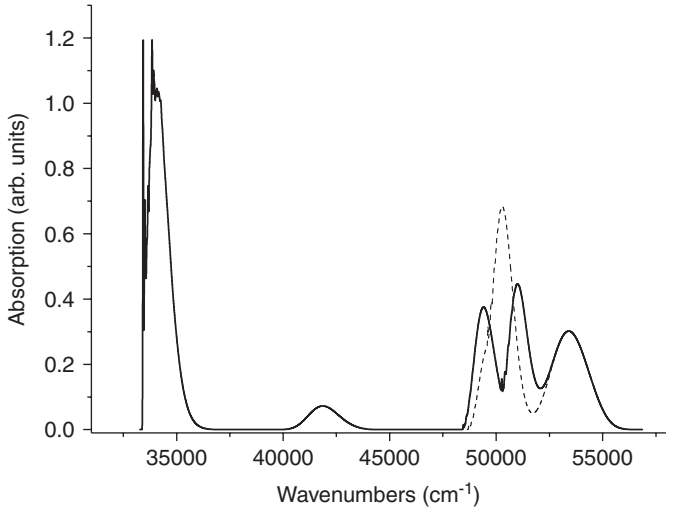

Fig. 1. Simulated unpolarized absorption in $LiYF_4:Ce^{3+}$ at $T = 0$. The dashed envelope was obtained without taking into account the interaction with the non-adiabatic phonons.

Thus, we can separate out three regions in the considered $4f^N$–$4f^{N-1}$5d absorption spectra (see Figs. 1, 2, 7) related to the lowest crystal field state of the 5d-electron (orbital singlet) weakly coupled to phonons, to the first excited 5d-state strongly coupled to adiabatic phonons, to the

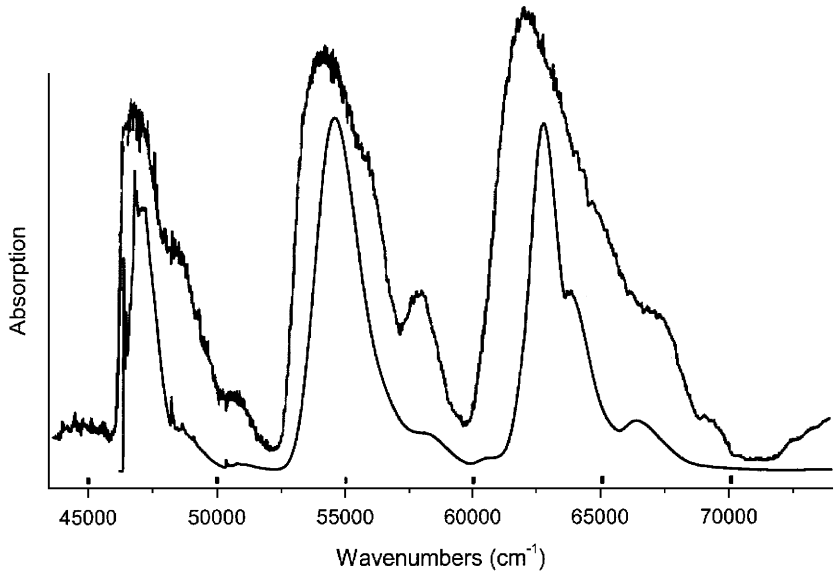

Fig. 2. Simulated unpolarized absorption from the ground state of Pr^{3+} in $LiYF_4$ (lower curve) and the excitation spectrum measured at $T = 6$ K [21] (upper curve).

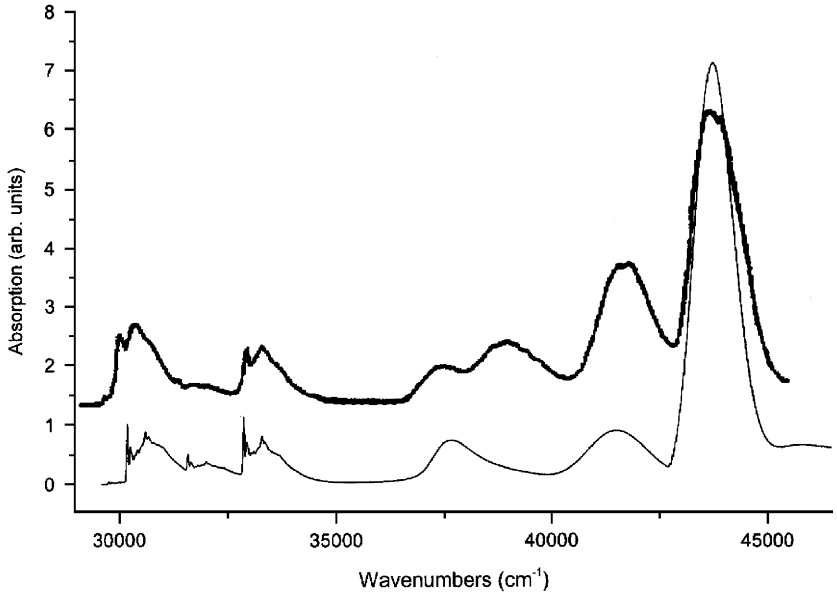

Fig. 3. Simulated (lower curve) and measured ($T = 8$ K) [20] (upper curve) σ-polarized absorption from the lowest crystal field sublevel of the $^1D_2$ multiplet in $LiYF_4$:Pr^{3+}.

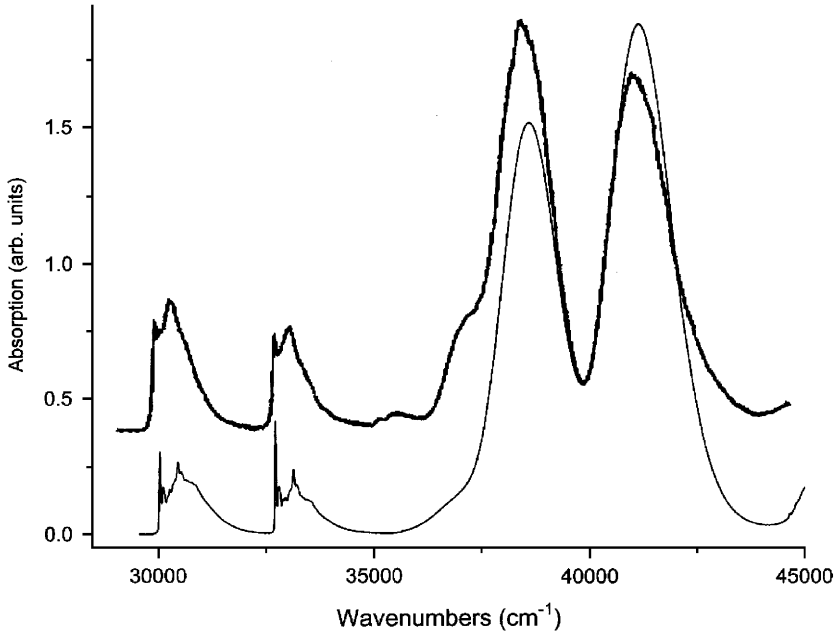

Fig. 4. Simulated (lower curve) and measured ($T = 8$ K) [20] (upper curve) π-polarized absorption from the lowest crystal field sublevel of the $^1D_2$ multiplet in $LiYF_4$:Pr^{3+}.

continuum of mixed electron–phonon states originated from the upper 5d-orbital doublet and the highest singlet, respectively. The Huang–Rhys parameters of the lower group of energy levels belonging to the $4f^{N-1}5d$ configuration are less than 3.5, the relaxation broadening of these levels does not exceed the broadening induced by random lattice strains, and only those absorption bands which correspond to transitions terminating on these levels exhibit a fine structure due to a relatively high weight of the one-phonon component (15) in the form-function (13). In particular, this fine structure is well resolved in the measured polarized absorption spectra from the excited states (ESA) of Pr^{3+} [20] and is well reproduced by simulations (see Figs. 3–6). In the 4f5d configuration, there are 19 levels with the Huang–Rhys parameters from 2.3 to 3.3 and energies up to 4200 cm^{-1} (from the lowest 4f5d state). The next group contains 20 levels with the Huang–Rhys parameters from 8 to 15.5 in the range of energies 4900–9900 cm^{-1}, transitions to these levels are represented by structureless wide bands with widths mainly determined by the adiabatic electron–phonon coupling. The remaining 65 levels are distributed in the range of

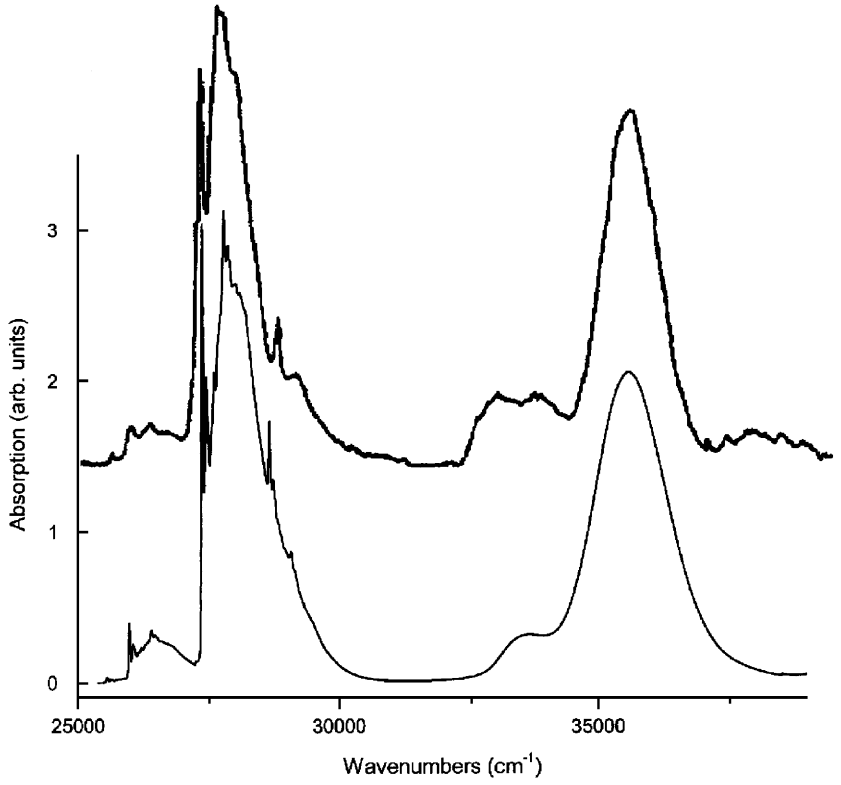

Fig. 5. Simulated (lower curve) and measured ($T = 8$ K) [20] (upper curve) σ-polarized absorption from the $^3P_0$ state of Pr^{3+} in $LiYF_4$.

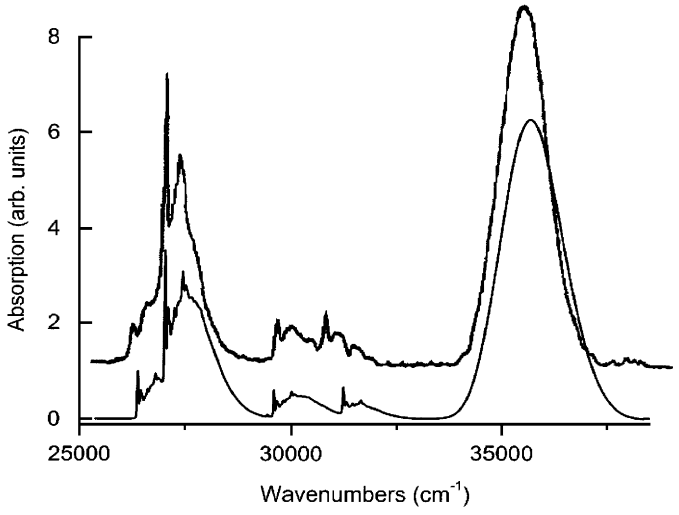

Fig. 6. Simulated (lower curve) and measured ($T = 8$ K) [20] (upper curve) π-polarized absorption from the $^3P_0$ state of Pr^{3+} in $LiYF_4$.

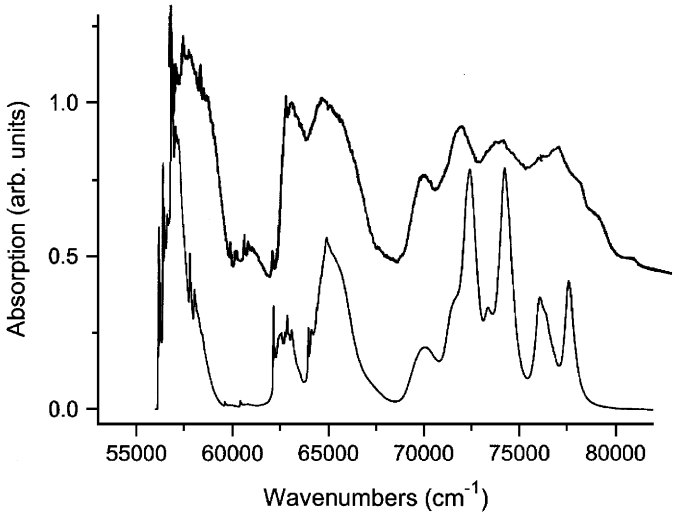

Fig. 7. Simulated unpolarized absorption in $LiYF_4$:Nd^{3+} (lower curve) and the measured excitation spectrum ($T = 6$ K) [21] (upper curve).

energies from 12,900 to 29,600 cm^{-1}, parameters $S(\Gamma)$ for these levels vary from 1.5 to 10. However, a small value of the Huang–Rhys parameter is the necessary, but not the sufficient condition for the presence of a fine structure. Due to strong interaction of these electronic states with the non-adiabatic phonons, the observed spectral density of the electric dipole transitions covers a much broader region as compared with the result of simulations in the framework of the adiabatic approximation (see Fig. 2, we have accounted for the splittings of the non-Kramers doublets but it is seen that this is not enough to reproduce widths of the measured bands). In the $4f^25d$ configuration values of $S(\Gamma)$ vary from 0.1 to 14, and energies of electronic states with relatively small values of the Huang–Rhys parameter are distributed in the wide range of 50,000 cm^{-1}. However, again only a lower group of 50 levels having values of $S(\Gamma) < 4$ and weakly mixed by non-adiabatic phonons, with energies up to 9000 cm^{-1} from the lowest state, gives rise to the fine structure in the spectral bands (see Fig. 7). Neglect of the configuration interaction, in particular, of the mixing

Table 3
Spectral parameters of impurity Ce^{3+} ions in $LiYF_4$

E_{CF} (cm^{-1})	E_{JT} (cm^{-1})	E (ZFL) (cm^{-1})	Frequency of the band maximum (cm^{-1})		Huang–Rhys parameter	Relative intensities of the GSA	
			Theory	Exper. [21]		$\pi(\varepsilon\|\|c)$	$\sigma(\varepsilon\|\|a)$
1	2	3	4	5	6	7	8
34219	−788	33431	34020	34000	3.37	1.412	3.106
41961	−2526	39435	41800	41670	15.14	0	0.310
49789	−1076	48713	49400	49260	6.67	0	0.610
50498	−884	49614	51000	51020	5.58	0.354	0.997
53535	−3234	50301	53400	53470	17.62	0.044	1.219

of the higher $4f^3$ states with the $4f^25d$ states, may be a reason for differences between the upper fragments of the calculated and measured spectra in Fig. 7, but, first of all, a derivation of the more rigorous theory of the non-adiabatic electron–phonon interaction remains a challenging problem.

Acknowledgments

The authors acknowledge the support from the Ministry of Education and Science of Russian Federation (project 2.1.1.7348) and from RFBR (Grant no. 03-02-16449). BZM is grateful to A.A. Kaplyanskii for encouraging collaboration over the many years and to M. Reid for discussions which have stimulated this work.

References

[1] P.P. Feofilov, Opt. Spectrosk. 1 (1956) 992.
[2] A.A. Kaplyanskii, P.P. Feofilov, Opt. Spectrosk. 13 (1962) 129; A.A. Kaplyanskii, P.P. Feofilov, Opt. Spectrosk. 13 (1962) 235.
[3] M. Wagner, W.E. Bron, Phys. Rev. A 139 (1965) A223; W.E. Bron, M. Wagner, Phys. Rev. A 139 (1965) A233.
[4] A.A. Kaplyanskii, A.K. Przhevuskii, Opt. Spectrosk. 19 (1965) 597; A.A. Kaplyanskii, A.K. Przhevuskii, Opt. Spectrosk. 20 (1966) 1045.
[5] W.M. Yen, L.R. Elias, D.L. Huber, Phys. Rev. Lett. 24 (1970) 1011.
[6] Wm.S. Heaps, L.R. Elias, W.M. Yen, Phys. Rev. B 13 (1976) 94.
[7] M.F. Reid, L. van Pieterson, A. Meijerink, J. Alloys Compounds 344 (2002) 240.
[8] K. Ogasawara, S. Watanabe, H. Toyoshima, T. Ishii, M.G. Brik, H. Ikeno, I. Tanaka, J. Solid State Chem. 178 (2005) 412.
[9] G.K. Liu, X.Y. Chen, N. Edelstein, M.F. Reid, J. Huang, J. Alloys Compounds 374 (2004) 240.
[10] M. Lax, J. Chem. Phys. 20 (1952) 1752.
[11] E.U. Condon, Phys. Rev. 32 (1928) 858.
[12] Yu.E. Perlin, B.S. Tzukerblat, Electron-Vibrational Interaction Effects on Optical Spectra of Impurity Paramagnetic Ions, Kishinev, Stiintza, 1974.
[13] M.A. Krivoglaz, S.I. Pekar, Proc. Institute Phys. AS USSR 4 (1953) 37.
[14] M.H.L. Pryce, Interaction of lattice vibrations with electrons at lattice defects, in: R.W.H. Stevenson (Ed.), Phonons, Plenum, New York, 1966 p. 403.
[15] E. Garcia, R.R. Ryan, Acta Crystallogr. C 49 (1993) 2053.
[16] S. Salaun, M.T. Fornoni, A. Bulou, M. Rousseau, P. Simon, J.Y. Gesland, J. Phys.: Condens. Matter 9 (1997) 6941.
[17] S. Salaun, A. Bulou, M. Rousseau, B. Hennion, J.Y. Gesland, J. Phys.: Condens. Matter 9 (1997) 6957.
[18] M.N. Popova, E.P. Chukalina, B.Z. Malkin, S.K. Saikin, Phys. Rev. B 61 (2000) 7421.
[19] B.Z. Malkin, in: G. Liu, B.B. Jacquier (Eds.), Spectroscopic Properties of Rare Earths in Optical Materials, Springer Series in Materials Science, 83, 2005, pp. 130–190.
[20] M. Laroche, J.-L. Doualan, S. Girard, J. Margerie, R. Moncorge, J. Opt. Soc. Am. B 17 (2000) 1291.
[21] L. van Pieterson, M.F. Reid, R.T. Wegh, S. Soverna, A. Meijerink, Phys. Rev. B 65 (2002) 045113.
[22] L. van Pieterson, M.F. Reid, G.W. Burdick, A. Meijerink, Phys. Rev. B 65 (2002) 045114.
[23] A. Collombet, Y. Guyot, M.F. Joubert, M. Laroche, J. Margerie, R. Moncorge, E. Descroix, Phys. Rev. B 68 (2003) 035115.
[24] P.S. Peijzel, P. Vergeer, A. Meijerink, M.F. Reid, L.A. Boatner, G.W. Burdick, Phys. Rev. B 71 (2005) 045116.
[25] B.Z. Malkin, in: A.A. Kaplyanskii, R.M. Macfarlane (Eds.), Spectroscopy of Solids Containing Rare-Earth Ions, Elsevier Science Publishers, Amsterdam, 1987 p. 13 (Chapter 2).
[26] N.V. Starostin, P.F. Gruzdev, E.P. Pashnina, V.A. Ganin, Spectroscopy of Crystals, Nauka, Moskva, 1975, p. 216.
[27] N.V. Starostin, Spectroscopy of Crystals, Nauka, Moskva, 1975, p. 12.
[28] E. Clementi, A.D. McLean, Phys. Rev. 133 (1964) A419.
[29] M. Stephan, M. Zachau, M. Groting, O. Karplak, V. Eyert, K.C. Mishra, P.C. Schmidt, J. Lumin. 114 (2005) 255.
[30] L.K. Aminov, B.Z. Malkin, M.A. Koreiba, S.I. Sakhaeva, V.R. Pekurovskii, Opt. Spectrosk. 68 (1990) 835.
[31] M.J. Lee, M.F. Reid, M.D. Faucher, G.W. Burdick, J. Alloys Compounds 323–324 (2001) 636.
[32] H. De Leebeeck, C. Görller-Walrand, J. Alloys Compounds 275–277 (1998) 407.
[33] P. Rambaldi, R. Moncorge, J.P. Wolf, C. Pedrini, J.Y. Gesland, Opt. Commun. 146 (1998) 163.
[34] T. Yosida, M. Yamaga, D. Lee, T.P.J. Han, H.G. Gallagher, B. Henderson, J. Phys.: Condens. Matter 9 (1997) 3733.
[35] P.S. Peijzel, P. Vergeer, A. Meijerink, M.F. Reid, L.A. Boatner, G.W. Burdick, Phys. Rev. B 71 (2005) 045116.
[36] N.Yu. Kirikova, M. Kirm, J.C. Krupa, V.N. Makhov, E. Negodin, J.Y. Gesland, J. Lumin. 110 (2004) 135.